Initial Coupling of Binding to Gating Mediated by Conserved Residues in the Muscle Nicotinic Receptor

Nuriya Mukhtasimova, Chris Free, and Steven M. Sine

Receptor Biology Laboratory, Department of Physiology and Biomedical Engineering, Mayo Clinic College of Medicine, Rochester, MN 55905

We examined functional consequences of intrasubunit contacts in the nicotinic receptor α subunit using single channel kinetic analysis, site-directed mutagenesis, and structural modeling. At the periphery of the ACh binding site, our structural model shows that side chains of the conserved residues αK145, αD200, and αY190 converge to form putative electrostatic interactions. Structurally conservative mutations of each residue profoundly impair gating of the receptor channel, primarily by slowing the rate of channel opening. The combined mutations αD200N and αK145Q impair channel gating to the same extent as either single mutation, while αK145E counteracts the impaired gating due to αD200K, further suggesting electrostatic interaction between these residues. Interpreted in light of the crystal structure of acetylcholine binding protein (AChBP) with bound carbamylcholine (CCh), the results suggest in the absence of ACh, αK145 and αD200 form a salt bridge associated with the closed state of the channel. When ACh binds, αY190 moves toward the center of the binding cleft to stabilize the agonist, and its aromatic hydroxyl group approaches αK145, which in turn loosens its contact with αD200. The positional changes of αK145 and αD200 are proposed to initiate the cascade of perturbations that opens the receptor channel: the first perturbation is of β-strand 7, which harbors αK145 and is part of the signature Cys-loop, and the second is of β-strand 10, which harbors αD200 and connects to the M1 domain. Thus, interplay between these three conserved residues relays the initial conformational change from the ACh binding site toward the ion channel.

The Journal of General Physiology

INTRODUCTION

Activation of post-synaptic receptors is accomplished by allosteric communication between the neurotransmitter binding site and the distal ion channel. The local conformational change due to neurotransmitter binding is amplified in a cascade that culminates in the global conformational change that opens the channel. For the Cys-loop superfamily of post-synaptic receptors, atomic-scale insight into the neurotransmitter binding site emerged from the x-ray structure of the homologous acetylcholine binding protein (AChBP; Brejc et al., 2001) and from homology models derived from it (Le Novere et al., 2002; Molles et al., 2002; Schapira et al., 2002; Sine et al., 2002a). Additionally a 4-Å resolution structural model of the binding, channel, and cytoplasmic domains was generated from electron microscopy of two-dimensional arrays of Torpedo receptors (Miyazawa et al., 2003; Unwin, 2005). At the interface between binding and pore domains, a network of loops was shown to couple neurotransmitter binding to channel gating (Kash et al., 2003; Bouzat et al., 2004; Chakrapani et al., 2004), but coupling structures near the neurotransmitter binding site remain unknown.

In the adult muscle nicotinic receptor, the two ACh binding sites are formed at interfaces between an α subunit and a neighboring ε or δ subunit where multiple recognition domains from each subunit converge (for reviews see Corringer et al., 2000; Karlin, 2002; Sine, 2002). The α subunit contributes recognition domains A–C, while the non-α subunit contributes domains D–G. Conserved aromatic residues from domains A–D form an aromatic cage that coordinates the positively charged agonist (Celie et al., 2004), whereas nonconserved residues in domains D–G endow the two binding sites with selectivity for agonists and competitive antagonists (Sine, 2002). Domains C and F are the most peripheral of the recognition domains, and of these, domain C exhibits the greatest displacement on binding the agonist (Celie et al., 2004; Gao et al., 2005).

To identify structures that propagate the local conformational change elicited by ACh away from the binding site, we examined our homology model of the receptor ligand binding domain (Sine et al., 2002a). We looked for conserved residues at the periphery of the binding site near the mobile domain C and found a cluster of three conserved residues, αK145, αD200, and αY190, whose side chains potentially interact through electrostatic forces. Our patch clamp recordings show that structurally conservative mutations of each residue profoundly impair gating of the channel. The common contributions to channel gating and direct linkages to the binding site and binding-pore interface suggest

Correspondence to Steven M. Sine: sine@mayo.edu

Abbreviations used in this paper: AChBP, acetylcholine binding protein; Btx, bungarotoxin; CCh, carbamylcholine.

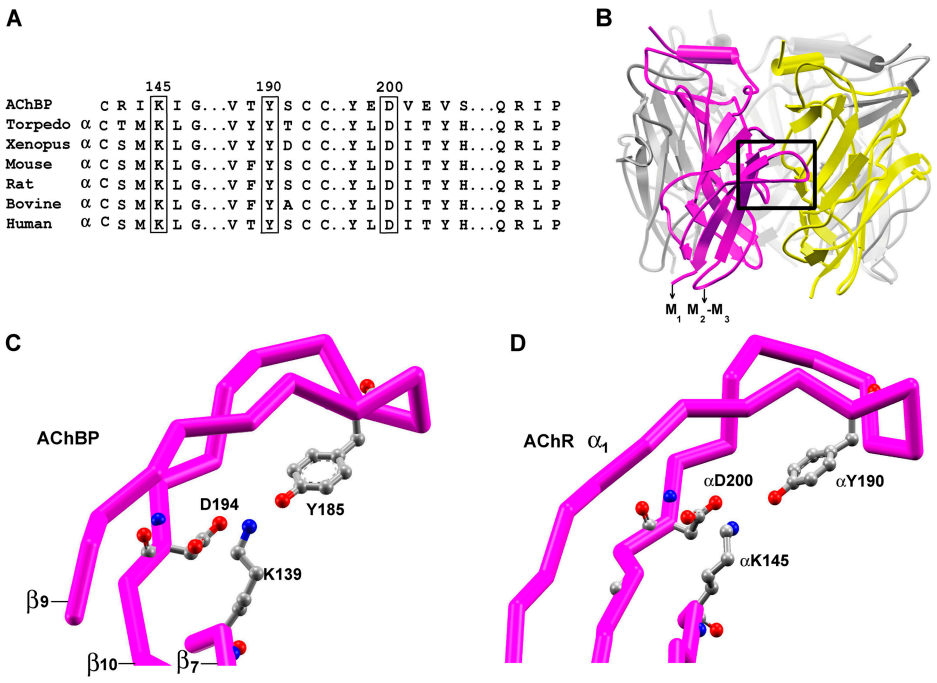

Figure 1. Sequence alignment and relationship between recognition domain C in AChBP and our structural model of receptor ligand binding domain. (A) Sequence alignment of residues in recognition domain C in AChBP and different species of α_1 subunits. Sequence numbers correspond to the α_1 subunit. Note the Cys-loop ends with the conserved Cys to the left, and the M1 domain starts with the conserved Pro to the right. (B) Mutagenesis-based homology model of the human muscle receptor ligand binding domain (Sine et al., 2002a). The α subunit is highlighted in magenta and ε subunit in yellow, with the remaining subunits in gray. The box encloses recognition domain C. Close up views of recognition domain C (β-strands 9–10) and underlying portion of the Cys-loop (β-strand 7) in AChBP (C) and receptor (D) with the triad of conserved residue side chains rendered in ball and stick representation.

interplay among these three residues initiates the allosteric cascade from the binding site to the channel gate.

MATERIALS AND METHODS

Construction of Wild-type and Mutant AChRs

Human α, β, ε, and δ subunit cDNAs were obtained as previously described (Ohno et al., 1996) and subcloned into the mammalian expression vector pRBG4 (Lee et al., 1991). Site-directed mutations were introduced using the Quick-Change site-directed mutagenesis kit (Stratagene). The presence of each mutation and the absence of unwanted mutation were determined by sequencing the entire cDNA insert.

Mammalian Cell Expression

BOSC 23 cells (Pear et al., 1993; Wang et al., 2000), a variant of HEK 293 clonal fibroblasts, were transfected with mutant or wild-type cDNAs using calcium phosphate precipitation as previously described (Lee and Sine, 2004). Patch clamp and [^{125}I]α-bungarotoxin (Btx) binding measurements were made 2 and 3 d after transfection, respectively.

Patch-clamp Recordings

Recordings were obtained in the cell-attached configuration (Hamill et al., 1981) at a membrane potential of −70 mV and a temperature of 21°C. Bath and pipette solutions contained 142 mM KCl, 5.4 mM NaCl, 1.8 mM $CaCl_2$, 1.7 mM $MgCl_2$, 10 mM HEPES (pH 7.4). Single channel currents were recorded using an Axopatch 200B (Axon Instruments Inc.). Data were obtained from two to four different patches for each ACh concentration. Recordings were accepted for analysis only when the frequency of occurrence of clusters of events was low enough to be sure they originated from a single receptor channel. Currents were low pass filtered at 100 kHz and recorded to hard disk at 200 kHz using the program Acquire (Bruxton Co.), using the option that allows high bandwidth sampling of periods of channel activity while keeping track of the intervening quiescent periods.

Single-channel Kinetic Analysis

Digitized current signals were analyzed as recently described (Lee and Sine, 2004) using a 10-kHz digital Gaussian filter, cubic spline interpolation of the signal, a dead time of 10 μs, the half-amplitude threshold for detection and correction of the measured dwell times at threshold for the effects of the Gaussian filter (Colquhoun and Sigworth, 1983). Dwell time histograms were constructed using a logarithmic abscissa and square root ordinate and fitted to the sum of exponential components by maximum likelihood using the program TACFit (Bruxton Co.). Clusters of events corresponding to a single channel were identified as a series of closely spaced openings preceded and followed by closed intervals greater than a specified duration. This duration was taken as the point of intersection of the closed time component that depended on ACh concentration with the succeeding closed time component due to desensitization. For analyses that included desensitized states, the closed duration for defining clusters was taken as the point of intersection of the closed time due to intermediate onset desensitization and the succeeding component determined by slow desensitization and the number of channels in the patch. Clusters of events with five or more openings and cluster mean open probabilities and cluster mean closed times within two standard deviations of the respective means were accepted for further analysis. Kinetic analysis was conducted simultaneously on data obtained across a range of ACh concentrations, termed global analysis, using MIL software (Qub suite, State University of New York, Buffalo), which corrects for missed events and gives error estimates of the fitted parameters (Qin et al., 1996). A dead time of 22 μs was imposed on all datasets. For each type of receptor studied, global analysis included data from two to four patches for each ACh concentration, ACh concentrations spaced at half-log unit intervals of the concentration, and a 10- to 333-fold range of the ACh concentration.

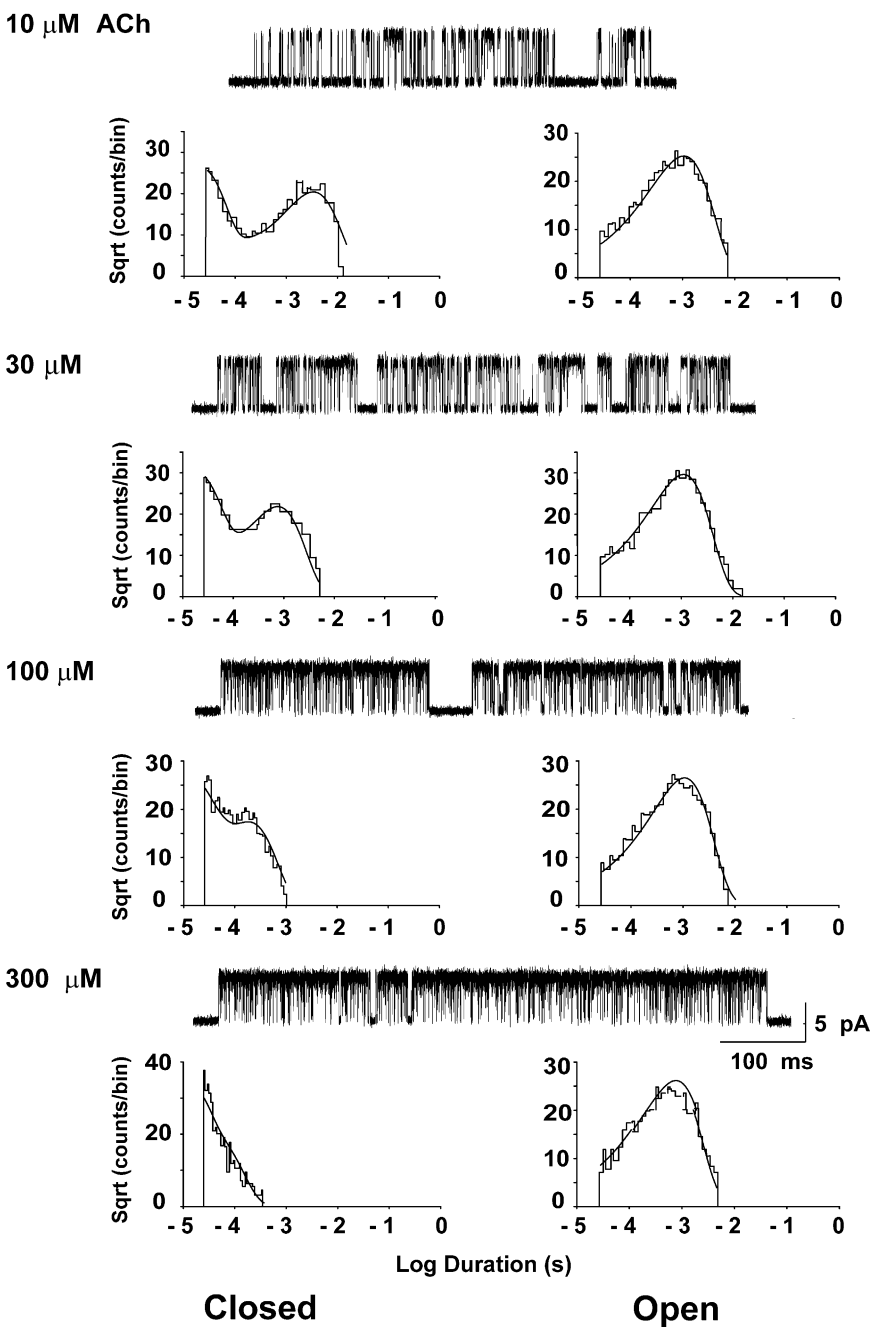

Figure 2. ACh-evoked single channel currents and kinetic analysis of adult human wild-type receptors in BOSC 23 cells. Individual clusters of single-channel currents recorded at the indicated concentrations of ACh are shown at a bandwidth of 10 kHz with openings displayed as upward deflections. Particularly long clusters are chosen to illustrate the change in activation kinetics at each ACh concentration. Histograms of closed and open durations for each ACh concentration are shown with probability density functions computed from the fitted Scheme I rate constants (see Table I) overlaid.

ACh Binding Measurements

The total number of [^{125}I]α-Btx binding sites on the cell surface of transfected BOSC 23 cells and ACh competition against the initial rate of [^{125}I]α-Btx were determined as previously described (Sine, 1993). ACh competition measurements were analyzed according to the following form of the Hill equation:

$$1 - Y = 1/[1 + ([ACh]/K_{app})^{n_H}],$$

where Y is fractional occupancy by ACh, n_H is the Hill coefficient, and K_{app} is the apparent dissociation constant.

RESULTS

Triad of Conserved Residues at the Periphery of the ACh Binding Site

Structures of AChBP and our homology model of the nicotinic receptor ligand binding domain show that recognition domain C is strategically positioned to transmit local conformational change due to ACh binding to structures linked to the ion channel (Fig. 1 B). Domain C comprises the loop spanning β-strands 9 and

10 of the α subunit and links directly to the M1 transmembrane domain via β-strand 10. It also overlays the Cys-loop, which articulates with the linker joining the M2 and M3 transmembrane domains (Kash et al., 2003; Bouzat et al., 2004; Unwin, 2005). Inspection of the AChBP structure, with and without carbamylcholine (CCh) bound, reveals two salt bridges that have counterparts in our structural model of the receptor ligand binding domain. At binding sites without CCh bound, a salt bridge forms between K139 and D194 of AChBP, whereas at binding sites with CCh bound, a salt bridge forms between K139 and Y185 (Celie et al., 2004; Fig. 1 C). In our structural model of the receptor ligand binding domain, residues equivalent to these, αK145, αD200, αY190, are close together in three-dimensional space and are conserved across all α_1 subunits (Figs. 1, A and D), suggesting key structural or functional contributions. Thus the x-ray structure of AChBP, our structural model of the receptor ligand binding domain and residue conservation together suggest that αK145, αD200, and αY190 are candidates for transmitting local conformational change at the ACh binding site to structures linked to the ion channel.

Single Channel Kinetics of the Adult Human Receptor

To provide a frame of reference for assessing the effects of receptor mutations, we recorded an independent set of ACh-evoked single channel currents for the adult human receptor under experimental conditions identical to those used to study the mutant receptors. We coexpressed α, β, ε, and δ subunits in BOSC 23 cells and recorded single channel currents using the cell-attached configuration of the patch clamp with defined concentrations of ACh in the patch pipette (see MATERIALS AND METHODS). Currents recorded at desensitizing concentrations of ACh consist of a series of clusters of closely spaced current pulses separated by prolonged quiescent periods (Sakmann et al., 1980; Sine and Steinbach, 1987; Colquhoun and Ogden, 1988). Channel events within each cluster correspond to activation of a single receptor channel, and exhibit an ACh-dependent shortening of closed periods between successive openings, with little ACh dependence of the open periods (Fig. 2). The corresponding closed dwell time histograms show a shift from long to short time of a major component of closings as the ACh concentration is increased, whereas the major component of openings is concentration independent.

To estimate rate constants for elementary steps underlying activation of a single receptor channel, we analyzed the global set of dwell times according to kinetic schemes (Fig. 3). Scheme I depicts receptor activation as sequential binding of ACh to the resting, closed receptor, followed by opening and then block by ACh of the doubly occupied open receptor. Scheme II contains

Scheme I.

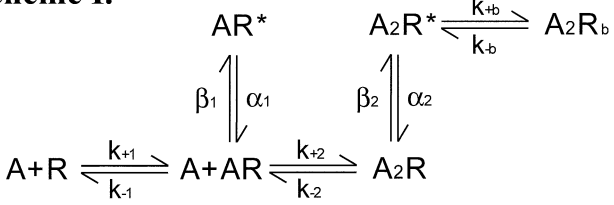

Scheme II.

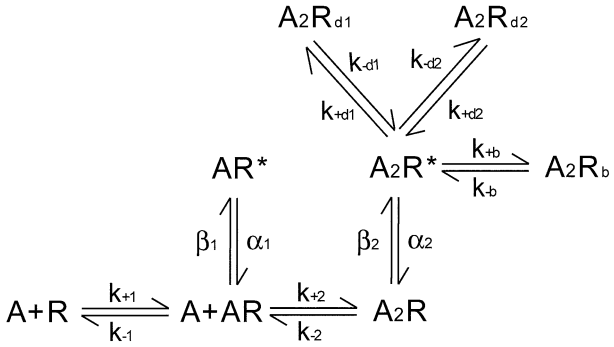

Figure 3. Kinetic schemes for receptor activation. Receptors in the resting closed state are symbolized by R, the open state by R*, and blocked state by R_b. ACh (A) associates with rate constants k_{+1}, k_{+2}, and k_{+b} and dissociates with rate constants k_{-1}, k_{-2}, and k_{-b}. Receptor channels open with rate constants β_1 and β_2, and close with rate constants α_1 and α_2. Scheme II incorporates fast and intermediate onset desensitized states with onset rate constants k_{+d1} and k_{+d2} and recovery rate constants k_{-d1} and k_{-d2}.

all of Scheme I but includes two desensitized states connected to the open state (Elenes and Auerbach, 2002; Lee and Sine, 2004). Scheme II is used to quantitatively account for the small fraction of closings due to fast and intermediate onset desensitization that are short enough to be indistinguishable from closings due to receptor activation. A third scheme depicting independent binding of ACh to each site, although able to describe data from the wild-type receptor (Hatton et al., 2003; Lee and Sine, 2004), is not applied here because it did not permit adequate definition of all the rate constants for the mutant receptors examined in this study.

Maximum likelihood fitting based on Scheme I yields probability density functions that describe the global set of closed and open dwell times for the adult human receptor (MATERIALS AND METHODS; Fig. 2). Rate constants underlying ACh binding, channel opening, and ACh blocking steps are all well defined by the analysis, and show rapid and efficient opening of the doubly occupied receptor, distinguishable association and dissociation rate constants for each binding site, and low affinity block of the open channel by ACh (Table I). The fitted rate constants are within the range of values previously reported for the adult human receptor (Ohno

TABLE I

Kinetics of Activation of AChRs Expressed in BOSC 23 Cells

Receptor	k_{+1}	k_{-1}	$K_1/\mu M$	k_{+2}	k_{-2}	$K_2/\mu M$	β_1	α_1	Θ_1	β_2	α_2	Θ_2	k_{+b}	k_{-b}	K_b/mM
Wild-type	346 ± 39	3480 ± 429	10	92 ± 2	19000 ± 355	207	65 ± 6	3500 ± 302	0.02	43000 ± 1046	2140 ± 41	20.1	33 ± 3	162000 ± 3790	4.9
Wild-type[a]	285 ± 37	2730 ± 390	9.6	81 ± 2	18900 ± 297	233	60 ± 6	4160 ± 436	0.014	42900 ± 1133	2070 ± 43	20.7	30 ± 3	161000 ± 3700	5.4
αK145A	154 ± 17	4900 ± 560	32	80 ± 9	9870 ± 1100	123	ND	ND	–	240 ± 40	1900 ± 20	0.13	18 ± 1	128000 ± 20200	7.1
αK145Q	105 ± 7	7150 ± 475	68	53 ± 3	14300 ± 950	269	ND	ND	–	734 ± 69	1670 ± 15	0.44	30 ± 2	106000 ± 9600	3.5
αD200N	275 ± 33	4200 ± 520	15	137 ± 16	8450 ± 1050	61	80 ± 9	14100 ± 1420	0.018	635 ± 112	2600 ± 40	0.24	28 ± 2	105000 ± 1700	3.8
αD200N + αK145Q	180 ± 16	4700 ± 410	26	90 ± 8	9400 ± 830	104	32 ± 5	7100 ± 900	0.0045	710 ± 90	1700 ± 19	0.42	26 ± 1	99000 ± 11900	3.8
αK145E	36 ± 2	3900 ± 300	108	18 ± 1	7730 ± 600	430	ND	ND	–	440 ± 50	1240 ± 15	0.35	29 ± 1	119000 ± 1100	4.1
αD200K[b]	–	–	–	–	–	–	–	–	–	105 ± 1	7600 ± 90	0.014	17 ± 0.2	130000 ± 5900	7.6
αD200K + αK145E	132 ± 17	4030 ± 500	31	66 ± 8	8060 ± 1000	122	40 ± 5	8160 ± 1000	0.01	490 ± 86	2520 ± 31	0.19	27 ± 3	114000 ± 20100	4.2
αD200K + αK145D	67 ± 10	1530 ± 200	23	34 ± 5	3050 ± 440	90	102 ± 6	4170 ± 130	0.024	183 ± 37	1730 ± 30	0.11	29 ± 2	101000 ± 20500	3.5
αT202V	360 ± 6	1420 ± 300	4	180 ± 3	28400 ± 640	158	ND	ND	–	27000 ± 860	1500 ± 32	18	32 ± 1	113000 ± 2500	3.5
αY190F[b]	–	–	–	–	–	–	–	–	–	42 ± 1	1690 ± 52	0.025	15 ± 1	113000 ± 2600	7.5
αY190F + αK145Q[b]	–	–	–	–	–	–	–	–	–	138 ± 4	1890 ± 23	0.073	30 ± 1	96700 ± 1300	3.2

Values are from global fits of Scheme I to data obtained over a range of ACh concentrations, with error limits given (see MATERIALS AND METHODS). Rate constants are in units of $\mu M^{-1}s^{-1}$ for association rate constants, and s^{-1} for all others. The channel gating equilibrium constants (Θ_n) are β_n/α_n. Ks are dissociation constants, k_-/k_+.

[a]Fits according to Scheme II, which contains two desensitized states linked to the open state (Fig. 3 and text). Fitted desensitization rate constants, (k_{+d1}/k_{-d1}) and (k_{+d2}/k_{-d2}) in units of s^{-1}, are D_1 (19/39), D_2 (24/660).

[b]Fits according to the subset of doubly occupied states in Scheme I. ND indicates parameters were not defined.

et al., 1996; Wang et al., 1999; Hatton et al., 2003; Lee and Sine, 2004).

Maximum likelihood fitting based on Scheme II, which incorporates brief and intermediate duration desensitized states, also describes the distributions of closed and open dwell times, and yields essentially the same rate constants for binding and gating steps obtained using Scheme I (Table I). The similar results obtained with Schemes I and II show that the presence of closings due to desensitization does not affect the estimates of rate constants for receptor activation when Scheme I is applied to the wild-type human receptor (Lee and Sine, 2004).

Functional Contribution of αK145

αK145 is a potential link between the binding site and the ion channel because it is proximal to the binding site, it is physically linked to the Cys-loop, it is proximal to electron-rich side chains that link to M1 via β-strand 10, and it is conserved across α_1 subunits. In the agonist-free structure of AChBP, the residue equivalent to αK145, K139, forms a salt bridge with D194, whereas in the CCh-bound structure, K139 forms a salt bridge with the key binding site tyrosine, Y185 (Celie et al., 2004). To investigate the functional contribution of αK145, we generated a series of mutations of αK145, coexpressed each with complementary β, ε, and δ subunits, and recorded ACh-evoked single channel currents.

Substitution of Ala for αK145 profoundly impairs receptor activation at all concentrations of ACh, with activation episodes due to a single receptor consisting of predominantly single openings separated by prolonged closings (compare Figs. 2 and 4). The corresponding closed time histograms span a wide range of times at all ACh concentrations examined, and the major peak of closings shows an ACh-dependent shift toward shorter times. Maximum likelihood fitting of Scheme I to the global dataset for αK145A well describes the closed and open dwell time histograms (Fig. 4). The fitted rate constants reveal nearly a 200-fold slowing of the channel opening rate constant and no change of the channel closing rate constant (Table I). For αK145A, adequate definition of the rate constants underlying ACh binding steps required the approximation that the set

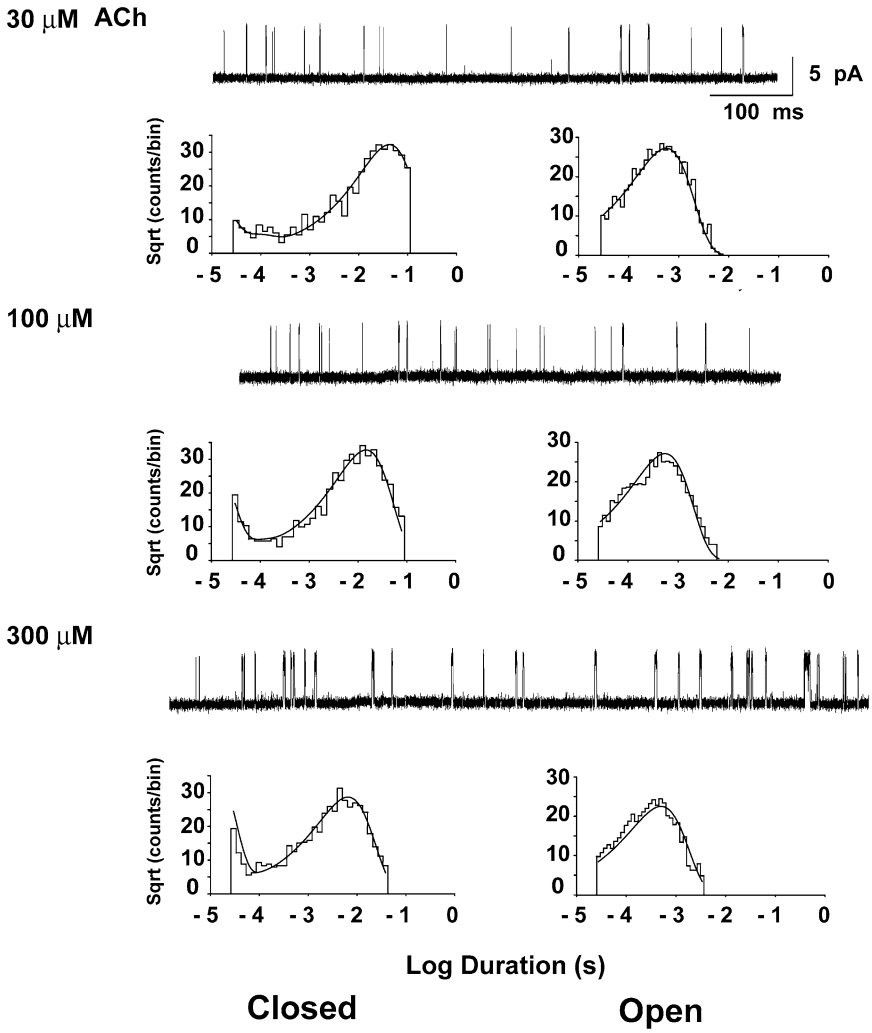

Figure 4. ACh-evoked single channel currents and kinetic analysis of receptors containing the mutation αK145A. Currents recorded at the indicated ACh concentrations are shown at a bandwidth of 10 kHz. Dwell time histograms are shown with pdfs generated from the Scheme I rate constants (Table I) overlaid.

of elementary association and dissociation rate constants are equal at each binding site. Presumably this approximation was required because information on the first binding step was limited: clusters of events corresponding to a single receptor could only be identified at ACh concentrations >30 μM, which may exceed the dissociation constant for ACh binding to the first binding site, and brief, mono-liganded openings were not present. Nevertheless, our analysis suggests that the rate constants underlying ACh binding are only modestly affected by αK145A (Table I). Thus substitution of Ala for αK145 at the periphery of the ACh binding site predominantly impairs elementary steps underlying channel gating.

Functional Consequences of αK145Q

Because the Lys to Ala substitution represents a substantial structural change, we examined functional consequences of the more structurally conservative mutation αK145Q. The Gln substitution neutralizes the positive charge but maintains polarity and moderate size of the side chain. Receptors containing αK145Q show impaired channel gating similar to αK145A, but individual activation episodes show three kinetic modes distinguished by low, intermediate, and high open probability (P_{open}; Fig. 5). These kinetic modes were observed only at high concentrations of ACh (300 μM to 1 mM), and although they were present at all high concentrations, the contributions of each mode varied from patch to patch. We therefore describe detection of the three kinetic modes for one patch to exemplify our treatment of the overall data for αK145Q.

We identified clusters of events corresponding to a single channel using our standard cluster discrimination method (MATERIALS AND METHODS), and generated histograms of mean cluster P_{open} and mean cluster

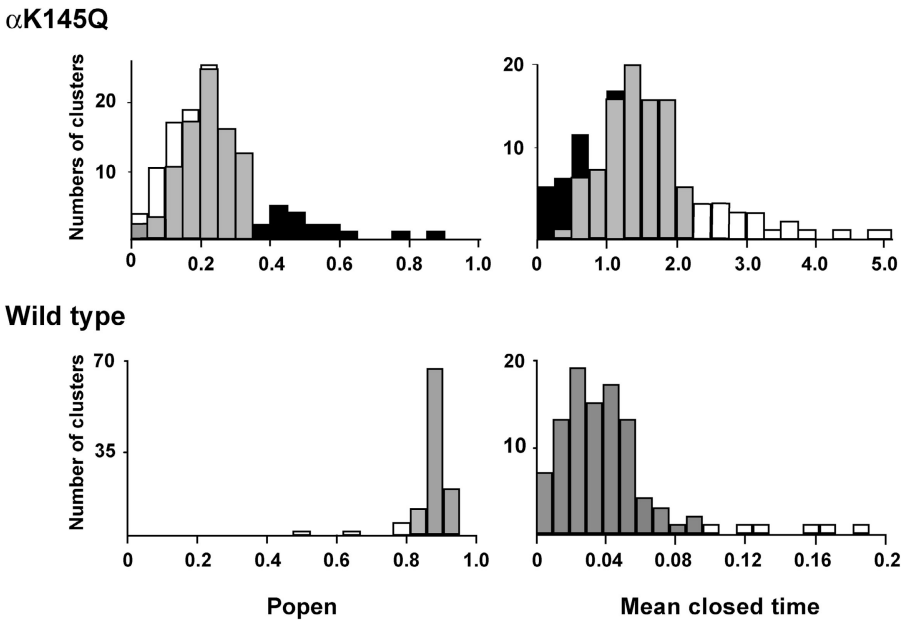

Figure 5. Detection of multiple kinetic modes for αK145Q receptors. Histograms of cluster P_{open} and mean closed time (τ_C) are shown for αK145Q and wild-type receptors activated by 1 mM ACh. Clusters were defined as a series of events flanked by closed times longer than the intersection of the closed time component due to fast desensitization with that of the major ACh concentration–dependent component (see MATERIALS AND METHODS; Lee and Sine, 2004). Kinetic modes were identified by correlating cluster P_{open} and τ_C; for αK145Q, the small peak with high P_{open} (filled bars) corresponds to clusters with short τ_C, the tail of long τ_C (open bars) corresponds to clusters with low P_{open}, and the remainder of the distributions corresponds to clusters with intermediate P_{open} and τ_C (gray bars). Note the same analysis applied to wild-type receptors reveals one predominant kinetic mode.

closed time (τ_C) for αK145Q (Fig. 5; Milone et al., 1998). The distribution of P_{open} shows a major and a minor peak, while the distribution of τ_C shows a major peak and a secondary tail of long τ_C. Analysis of cluster properties reveals that distinct portions of the two distributions are correlated: the peak of high P_{open} corresponds to clusters with short τ_C (filled bars), and the tail with long τ_C corresponds to clusters with low P_{open} (open bars). The remainder of the distributions consists of clusters with intermediate P_{open} and τ_C (gray bars). Clusters from wild-type receptors subjected to the same analysis show a predominant mode of high P_{open} and short τ_C.

We then separated clusters of events for each of the kinetic modes for αK145Q receptors, and combined one mode at a time with the kinetically homogeneous data obtained at lower ACh concentrations. Maximum likelihood fitting showed that only clusters with intermediate P_{open} and τ_C were compatible with data obtained at lower ACh concentrations. Fitting Scheme I to the intermediate mode dataset (30 μM to 1 mM ACh) shows that substitution of Gln for αK145 profoundly impairs the efficiency of channel gating; the corresponding probability density functions adequately describe the distributions of closed and open dwell times (Fig. 6). The effects of αK145Q on channel gating are similar to those of αK145A, with the channel opening rate constant slowed 60-fold and the channel closing rate constant relatively unchanged (Table I). Adequate definition of rate constants underlying ACh binding steps again required the approximation that the set of elementary association and dissociation rate constants are equal at each binding site. Given this approximation, the analysis suggests αK145Q has relatively little effect on agonist binding (Table I). Thus, located at the periphery of the ACh binding site, αK145 contributes primarily to gating of the receptor channel, fulfilling an important criterion as a transduction element.

Functional Contribution of αD200

αD200 is a potential electrostatic partner of αK145, and in the mouse receptor was found to contribute predominantly to channel gating (Akk et al., 1996). To determine whether αD200 contributes to channel gating in the human muscle receptor, and further, whether its functional contribution mirrors that of αK145, we recorded currents from adult human receptors harboring the mutation αD200N. Like mutations of αK145, αD200N profoundly impairs receptor activation at all concentrations of ACh; individual clusters consist of predominantly single openings interspersed by long closings (Fig. 7). Maximum likelihood fitting according to Scheme I reveals a predominant effect on channel gating, with the channel opening rate constant slowed nearly 70-fold and the channel closing rate constant slightly increased (Table I). As observed for mutations of αK145, adequate definition of rate constants underlying ACh binding steps required the approximation that the set of elementary association and dissociation rate constants are equal at each binding site. The rate constants underlying ACh binding are relatively unaffected by αD200N, as observed for the same mutation in the mouse receptor (Table I). Thus the consequences of αD200N for channel gating are highly similar between mouse and human receptors, and, moreover, mirror the consequences of mutations of αK145. The similar effects of mutations of αK145 and αD200

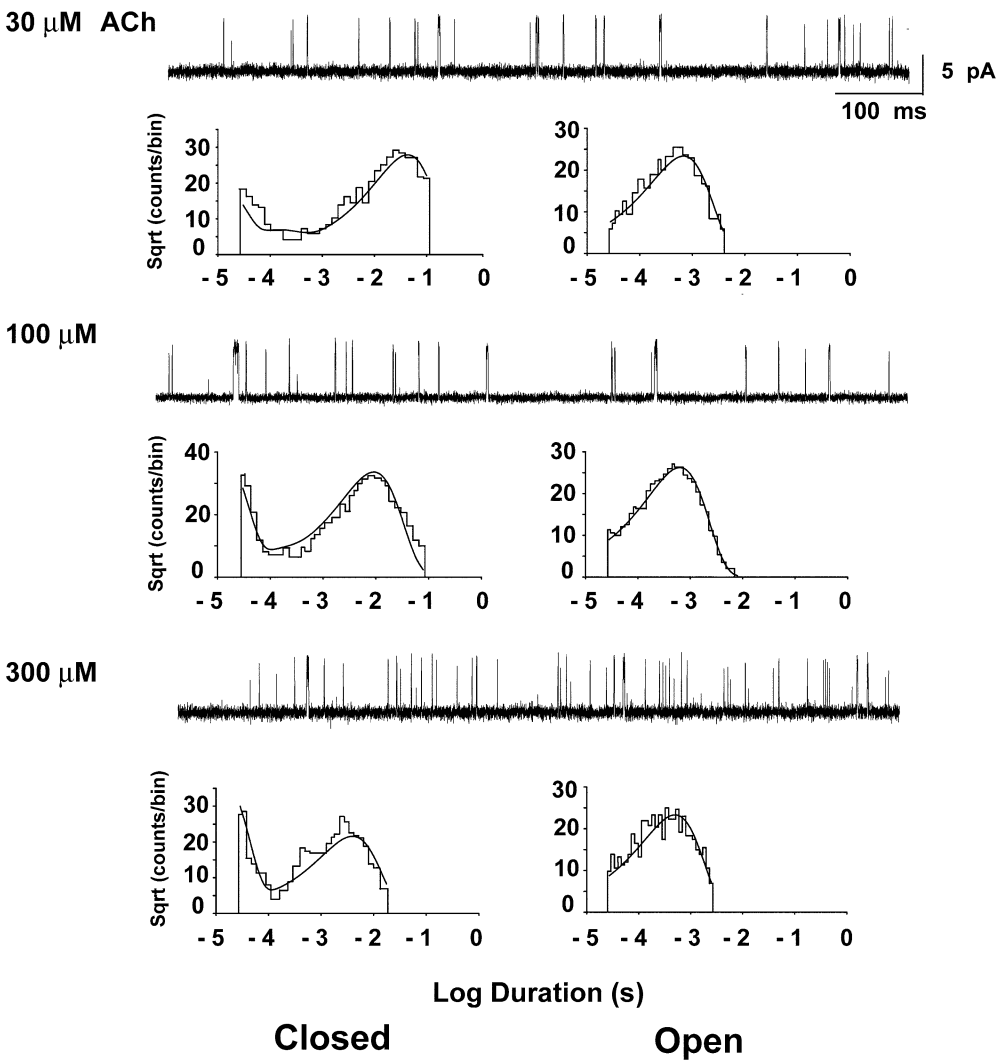

Figure 6. ACh-evoked single channel currents and kinetic analysis of the intermediate kinetic mode for receptors containing the mutation αK145Q. Currents from the intermediate mode at the indicated ACh concentrations are shown at a bandwidth 10 kHz. Dwell time histograms are shown with pdfs generated from the Scheme I rate constants (Table I) overlaid. Note the similar activation kinetics to those of αK145A.

on channel gating and proximity of the two side chains in our structural model collectively suggest these residues are interdependent and constitute part of an intermediate link between binding and gating domains.

Interdependence of αK145 and αD200

To gain additional evidence for interdependence of αK145 and αD200, we combined the mutations αK145Q and αD200N into a single α subunit and recorded ACh-evoked single channel currents from the resulting double mutant receptors. The current traces again show impaired receptor activation at all ACh concentrations (Fig. 8), with predominantly single openings separated by long closings, similar to either single mutation (compare Figs. 6, 7, and 8). Unlike receptors containing αK145Q alone, only a single kinetic mode was distinguished for the double mutant receptor, simplifying the analysis. Maximum likelihood fitting of Scheme I to the global set of dwell times reveals a 60-fold slowing of the channel opening rate constant and little change of the channel closing rate constant when compared with the wild-type receptor (Table I). These results are similar to those for either single mutation, showing qualitatively that αK145Q and αD200N are interdependent in contributing to channel gating. Double mutant cycles analysis (Horovitz and Fersht, 1990) applied to the set of gating equilibrium constants for wild-type, αK145Q, αD200N, and double mutant receptors yields a free energy of interaction of −2.6 kcal/mol. Rate constants underlying ACh binding steps are altered twofold or less by the double mutation, similar to αD200N alone, but this conclusion remains provisional because the assumption of equivalent binding sites was required to obtain well-defined rate constants.

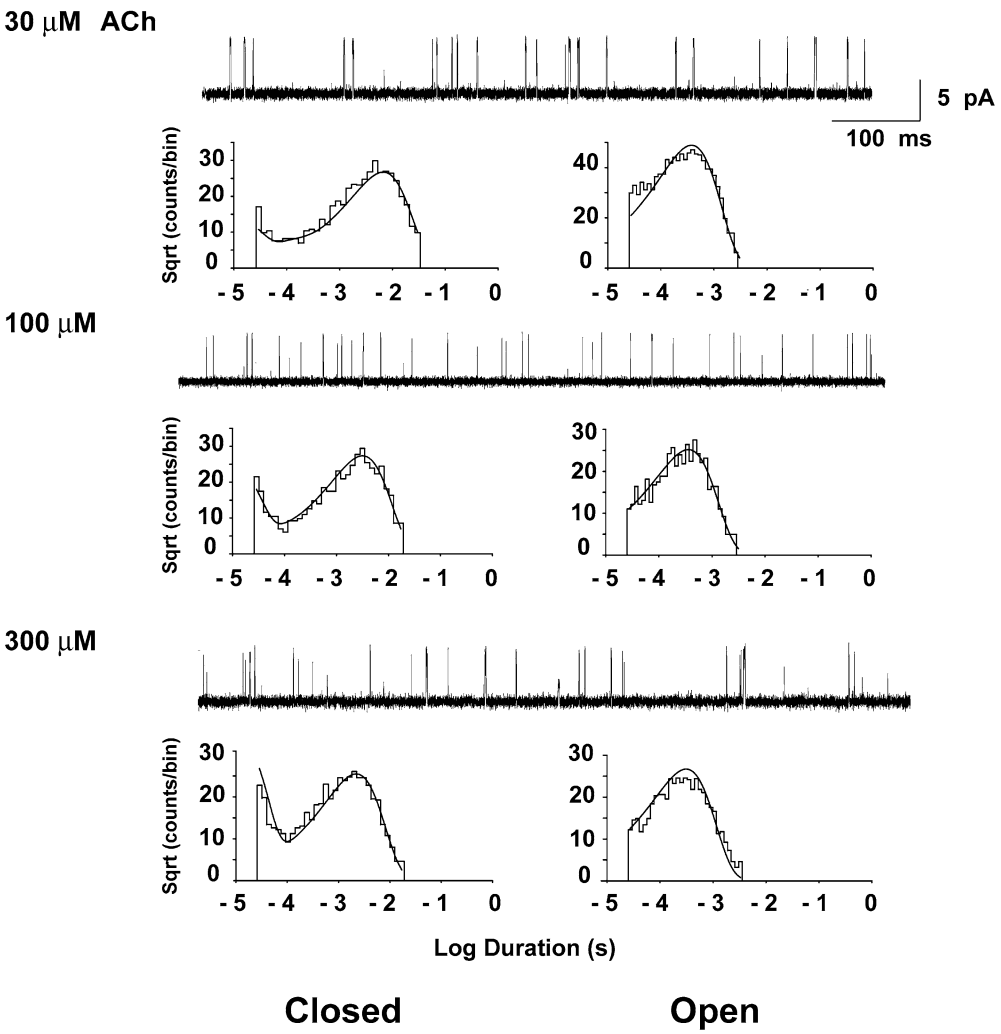

Figure 7. ACh-evoked single channel currents and kinetic analysis of receptors containing the mutation αD200N. Currents recorded at the indicated ACh concentrations are shown at a bandwidth 10 kHz. Dwell time histograms are shown with pdfs generated from the Scheme I rate constants (Table I) overlaid. Note the similar activation kinetics to those of αK145A and αK145Q.

Thus, the largely selective perturbation of channel gating by the double mutation quantitatively mirrors that for either single mutation, further suggesting αK145 and αD200 are interdependent in coupling agonist binding to channel gating.

Charge Reversal of αK145 and αD200

To test for electrostatic interaction between αK145 and αD200, we generated the single mutants αK145E and αD200K and the corresponding double mutant and recorded ACh-evoked single channel currents from the resulting mutant receptors (Fig. 9). The single mutation αD200K slows the channel opening rate constant 400-fold and increases the channel closing rate constant nearly fourfold, yielding a 1,400-fold decrease of the channel gating equilibrium constant (Table I). For αD200K, well-defined single receptor clusters could not be discerned at ACh concentrations <1 mM, preventing estimation of rate constants underlying ACh binding. Consequences of the single mutation αK145E mirror those of other mutations of αK145; compared with the wild-type receptor, the channel opening rate constant slows 100-fold, the channel closing rate constant slows almost twofold, and the ACh dissociation rate constants are only modestly affected. The rate constants for ACh association, on the other hand, slow three- to fivefold compared with other mutations of αK145 (Table I).

Compared with αD200K alone, restoring the local negative charge by combining αK145E markedly increases the frequency of channel openings within single receptor clusters (Fig. 9), and counteracts the slowing of the channel opening rate constant and the increase of the channel closing rate constant (Table I). The extent to which the gating rate constants are restored is only partial, perhaps because residues flanking each member of the putative salt bridge are not compatible with the reversed charge. The net result of

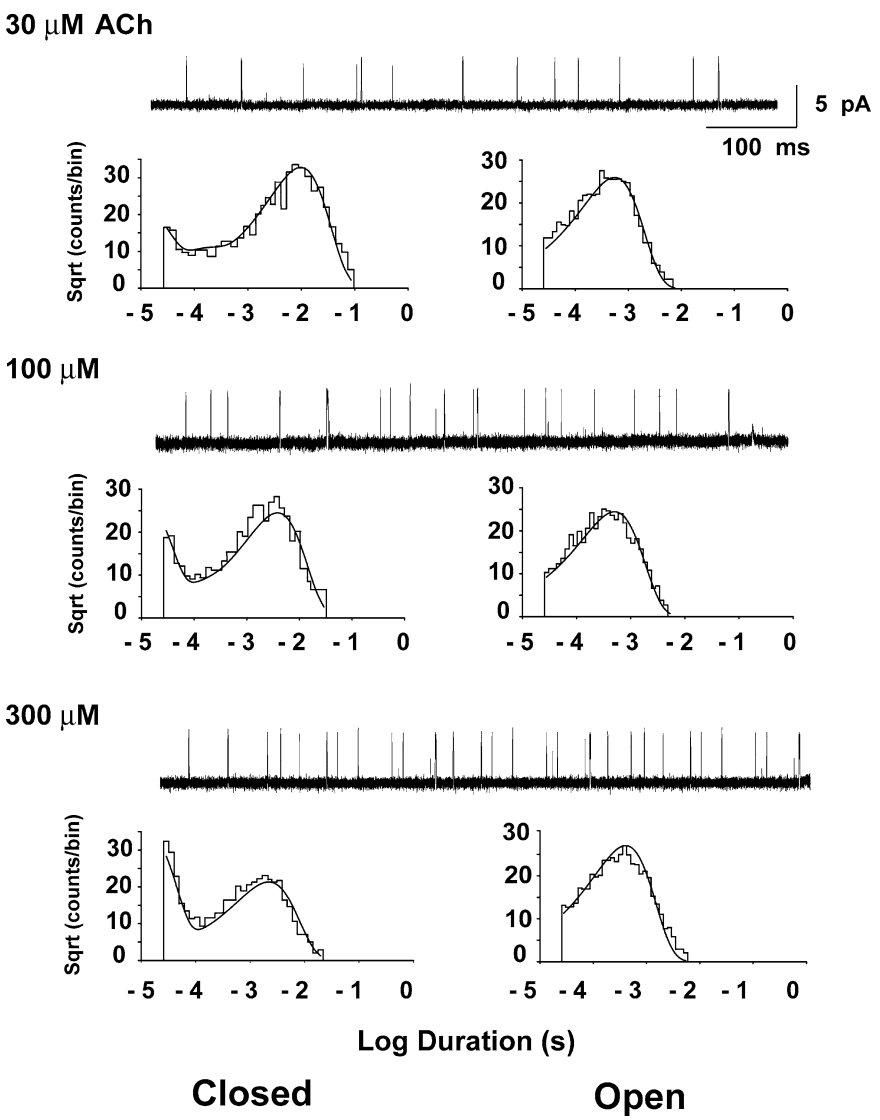

Figure 8. Charge neutralization of αK145 and αD200. ACh-evoked single channel currents and kinetic analysis are shown for the corresponding double mutant receptors. Currents recorded at the indicated ACh concentrations are shown at a bandwidth 10 kHz. Dwell time histograms are shown with pdfs generated from the Scheme I rate constants (Table I) overlaid. Note the similar activation kinetics to those of αK145Q and αD200N.

charge reversal is a 14-fold increase of the channel gating equilibrium constant compared with αD200K alone. Double mutant cycles analysis applied to the set of four gating equilibrium constants yields a free energy of interaction of −4 kcal/mol. Further, the slow association of ACh caused by αK145E alone is restored to the range of values observed for other mutations of αK145 (Table I).

Finally, we examined the single mutation αK145D and found that it prevented expression of functional channels and cell-surface α-Btx binding sites. However, αK145D is rescued by the charge reversal mutation αD200K. Full kinetic analysis of the double mutation reveals an eightfold increase of the channel gating equilibrium constant compared with αD200K alone, due to a twofold increase of the channel opening rate constant and a fourfold slowing of the channel closing rate constant (Table I). Changes in rate constants underlying ACh binding remain unknown because these could not be measured for either single mutation. However, the ACh association rate constants for the double mutation increase twofold compared with αK145E alone, while the ACh dissociation rate constants slow twofold compared with αK145E. The overall results from charge-neutralization and charge-reversal experiments provide strong evidence that αK145 and αD200 interact through electrostatic forces to couple agonist binding to channel gating.

Functional Contributions of αY190 and αT202

Our structural model predicts that two more residues are proximal to αK145 and αD200: αY190 and αT202

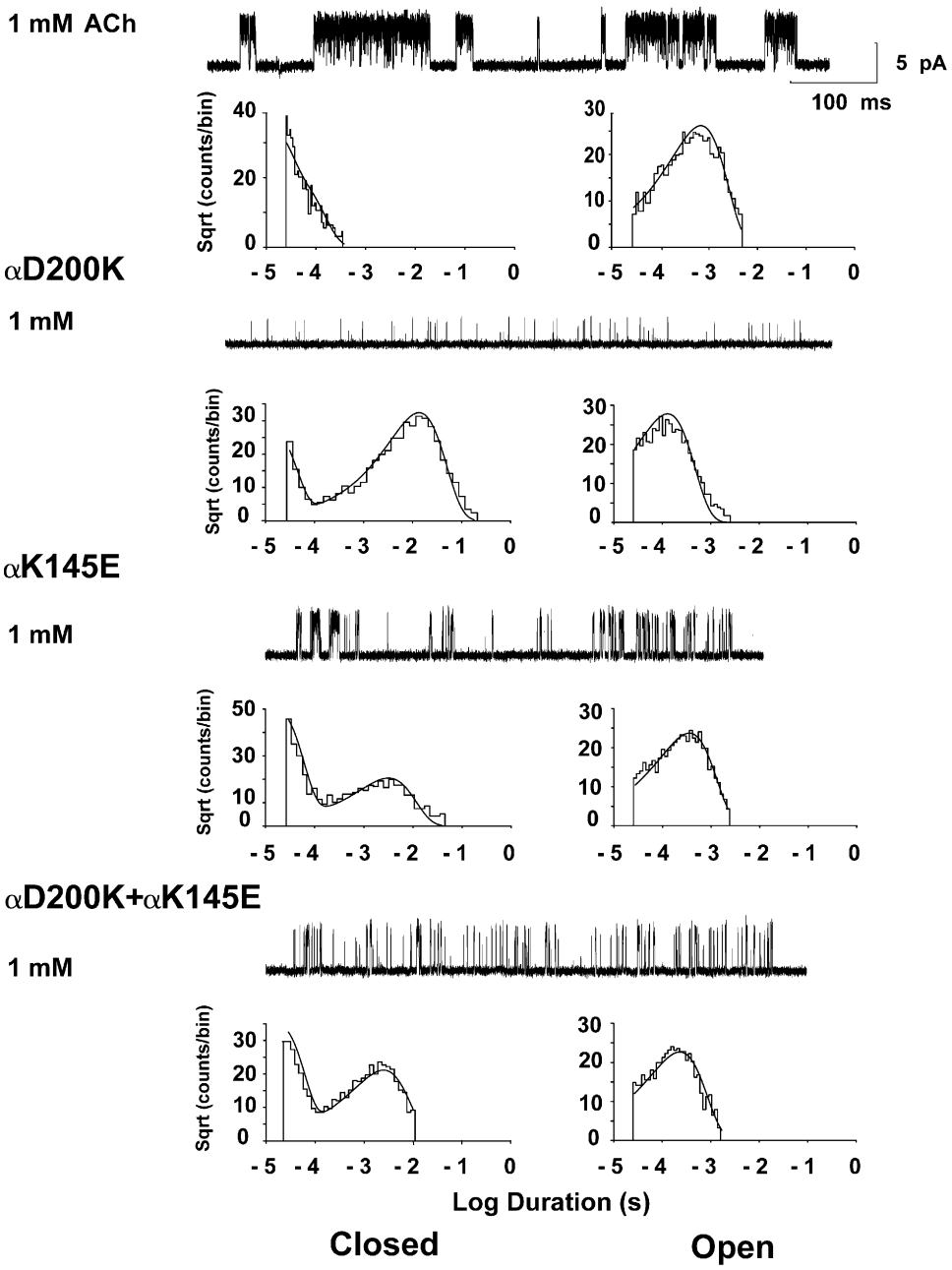

Figure 9. Charge reversal of αK145 and αD200. ACh-evoked single channel currents and kinetic analysis are shown for the single mutant and corresponding double mutant receptors. Currents recorded at the indicated ACh concentrations are shown at a bandwidth 10 kHz. Dwell time histograms are shown with pdfs generated from the Scheme I rate constants (Table I) overlaid. Note only the indicated saturating concentration of ACh produced clear-cut clusters of events for αD200K, allowing assignment of only channel gating and channel blocking rate constants. However the full set of Scheme I rate constants was obtained for αK145E and the charge reversal mutant (Table I). The charge reversal mutation increases the frequency of openings compared with αD200K alone.

(Fig. 1). We therefore generated structurally conservative mutations of each residue, αY190F and αT202V, and recorded single channel currents from the resulting mutant receptors. For receptors containing αY190F, the ACh concentration had to be increased to 3 mM to obtain well-defined clusters of single receptor currents; the corresponding intracluster events consist of single brief openings separated by prolonged closings (Fig. 10). The availability of data at only a single high concentration of ACh limited kinetic fitting to the subset of doubly occupied gating steps in Scheme I, but nevertheless reveals a 1,000-fold slowing of the channel opening rate constant with little change in the channel closing rate constant (Table I). These effects of αY190F on channel gating are analogous to those observed for the same mutation in the fetal mouse muscle receptor (Chen et al., 1995), but the 800-fold decrease of the gating equilibrium constant for the adult human receptor exceeds the 200-fold decrease observed for the fetal mouse receptor.

The kinetics of receptor activation are only modestly affected by αT202V. Rate constants for elementary

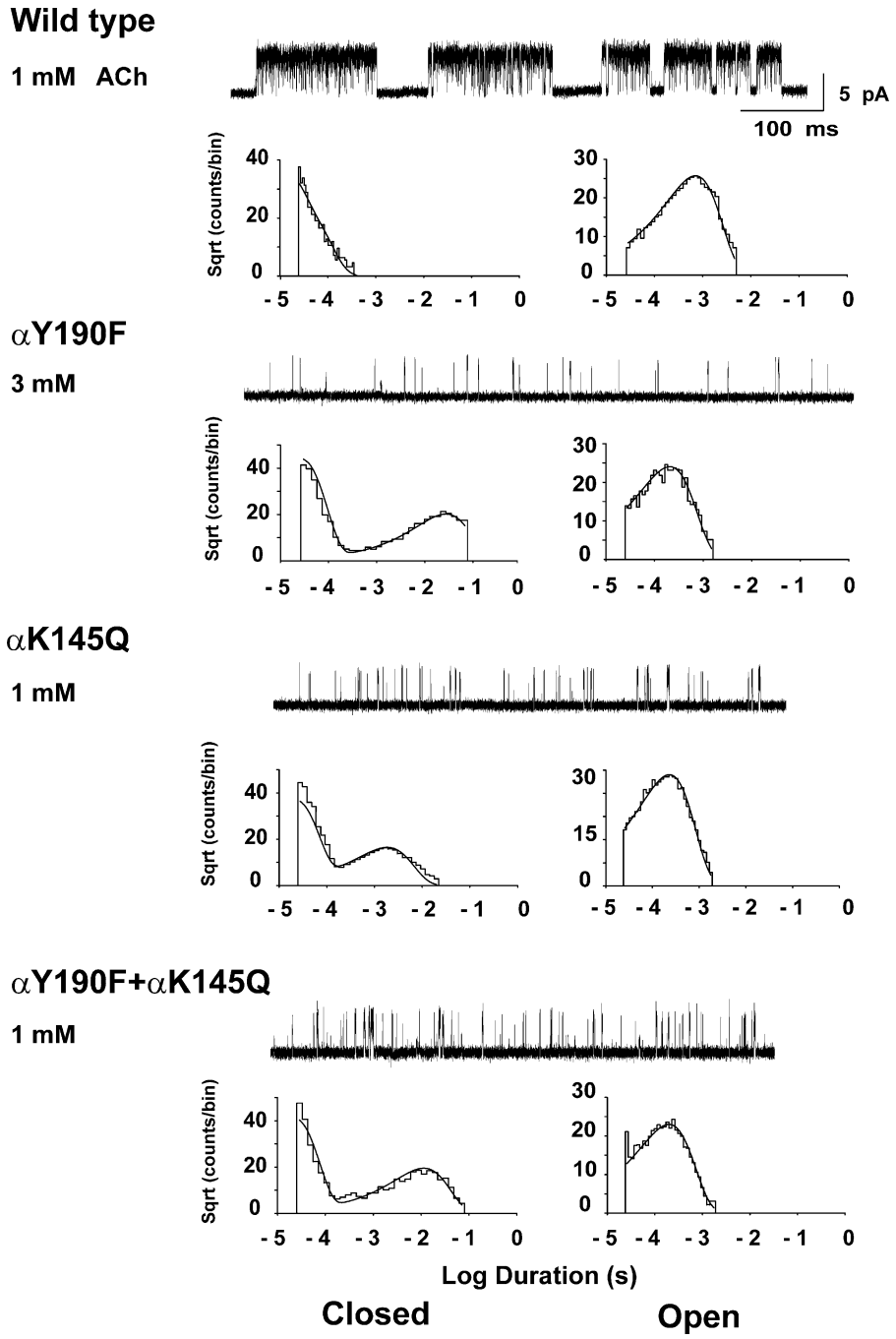

Figure 10. Kinetic consequences of αY190F and interdependence of αK145 and αY190. Currents recorded at the indicated ACh concentrations are shown at a bandwidth of 10 kHz for each mutant receptor. Dwell time histograms are shown with pdfs generated from the fitted rate constants underlying channel gating and ACh blocking steps in Scheme I (Table I) overlaid.

binding or gating steps change twofold or less compared with the wild-type receptor (Table I). Thus despite its conservation across α_1 subunits and proximity to αD200 and αK145, αT202 does not contribute substantially to either ACh binding or channel gating.

Interdependence of αK145 and αY190

The agonist-bound conformation of AChBP shows that K139 and Y185 form a salt bridge (Celie et al., 2004). To determine whether residues in the receptor equivalent to these, αK145 and αY190, are interdependent, we combined αK145Q and αY190F into a single α subunit and recorded ACh-evoked single channel currents from the resulting double mutant receptors. The current traces again show impaired receptor activation at 1 mM ACh, with brief openings separated by long closings, similar to either single mutation (Fig. 10). Unlike receptors containing αK145Q alone, only a single kinetic mode could be distinguished for the double mutant receptor. Further, well-defined clusters of single receptor openings could only be discerned at ACh concentrations from 100 μM to 1 mM, restricting the

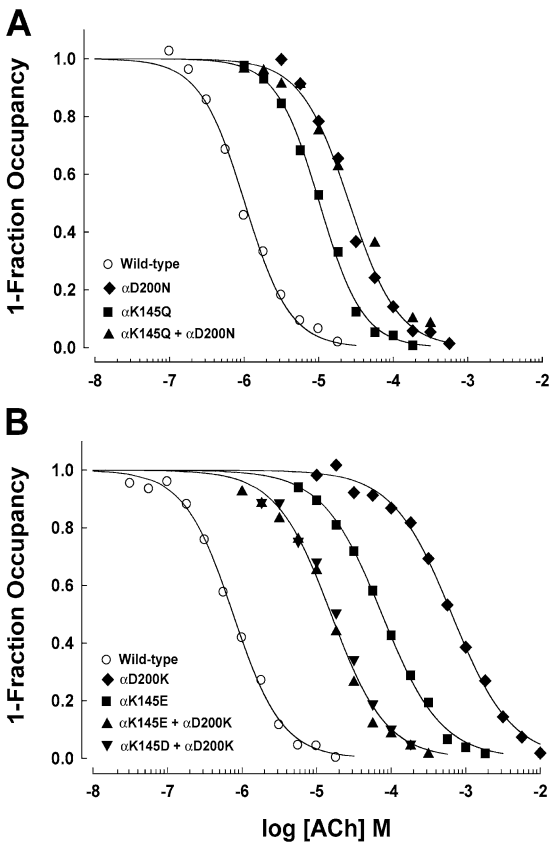

Figure 11. Steady-state binding of ACh to cell surface receptors with charge-neutral (A) and charge-reversal (B) mutations (see MATERIALS AND METHODS). Curves are fits to the Hill equation with the overall mean values of K_{app} and n_H given in Table II.

analysis to the channel gating rate constants. Maximum likelihood fitting shows that compared with the wild-type receptor, the double mutation slows the channel opening rate constant 200-fold without affecting the channel closing rate constant (Table I). Double mutant cycles analysis applied to the set of gating equilibrium constants for wild-type, αK145Q, αY190F, and double mutant receptors yields a free energy of interaction of −2.9 kcal/mol. Thus αK145Q and αY190F are interdependent in coupling agonist binding to channel gating.

Pairwise Interdependence Assessed by Steady-state Binding of ACh

Most mutations that affect receptor function alter steady-state binding of ACh (examples include Chen et al., 1995; Ohno et al., 1996; Sine et al., 2002b). Although measurements of steady-state ACh binding contain contributions from closed, open, and desensitized states of the receptor, each of which differs in affinity for the agonist (Katz and Thesleff, 1957; Sine and Taylor, 1979; Jackson, 1989), binding measurements can be used as an overall index of receptor function. We therefore sought further evidence for pairwise interdependence by measuring steady-state binding of ACh to receptors containing single and double mutations. We first studied the charge neutral mutations αK145Q and αD200N and the corresponding double mutation. Relative to the wild-type receptor, the single mutations αK145Q and αD200N increase the apparent dissociation constant for ACh (K_{app}) 10- and 26-fold, respectively, qualitatively consistent with expectations from impaired channel gating observed by single channel recording (Fig. 11; Table II). The double mutation shows a virtually identical binding profile to that of αD200N alone, and double mutant cycles analysis applied to K_{app} yields an interaction free energy of 1 kcal/mol for this charge neutralization experiment. Like K_{app}, interaction free energy based on K_{app} arises from multiple processes: ACh binding, desensitization, and channel gating. One of these processes is channel gating, which contributes 2.6 kcal/mol, but the other processes likely contribute. We next measured steady-state ACh binding for the charge reversal mutations αK145E and αD200K and the corresponding double mutation. The single mutations αK145E and αD200K increase K_{app} 100- and 860-fold, respectively, again qualitatively consistent with profoundly impaired channel gating (Fig. 11; Table II). However, charge reversal by the double mutation strongly counteracts the effects of either single mutation, yielding an overall 20-fold increase of K_{app} compared with the wild-type receptor. Double mutant cycles analysis applied to K_{app} for this charge reversal experiment reveals an interaction free energy of 4.8 kcal/mol, which is similar to the contribution of 4 kcal/mol observed for channel gating alone. The mutation αK145D does not produce functional receptors, but when combined with αD200K, yields a K_{app} coincident with that obtained for αK145E plus αD200K (Fig. 11; Table II).

The double mutation containing αK145Q and αY190F failed to bind α-Btx, preventing assessment of interdependence by steady-state ACh binding. Nevertheless the overall results provide strong evidence for electrostatic interaction between αK145 and αD200 and interdependence of αK145 and αY190. A three-way electrostatic interplay of charged residues thus emerges as a compelling candidate for an initial link between ligand binding and channel gating domains owing to the proximity of the triad to the ACh binding site, interdependence of residues in the triad, connections to the Cys-loop and M1 domain, and the predominant contributions of all three residues to channel gating.

Subunit Specificity of the Mutations

The three residues studied here are unique to and conserved across α_1 subunits. However, δ subunits also contain conserved Asp and Lys at positions equivalent to αD200 and αK145, respectively. To determine whether

TABLE II

Steady-state ACh Binding to Receptors Expressed on Intact BOSC 23 Cells

Receptor	No. of determinations	$K_{app}/\mu M$	n_H
Wild-type	16	1.0 ± 0.2	1.3 ± 0.2
αK145A	2	53 ± 4.6	1.1 ± 0.1
αK145Q	8	10 ± 4.6	1.1 ± 0.2
αD200N	6	15 ± 4.8	1.0 ± 0.1
αD200N + αK145Q	4	31 ± 10	1.0 ± 0.16
αK145E	3	84 ± 18	1.3 ± 0.5
αD200K	3	390 ± 34	1.0 ± 0.2
αD200K + αK145E	3	12 ± 2.3	1.4 ± 0.1
αD200K + αK145D	3	13 ± 5.2	1.4 ± 0.2
αT202V	1	2.5 ± 0.3	1.0 ± 0.2
αY190F	3	900 ± 330	1.1 ± 0.1
δK147Q	2	1.0 ± 0.3	1.2 ± 0.1
δD214N	2	0.6 ± 0.1	1.0 ± 0.03

For each type of receptor, mean values and standard deviations are given for the indicated number of experiments.

this residue pair in the δ subunit contributes to receptor function, we generated the mutations δK147Q and δD214N, coexpressed each with complementary α, β, and ε subunits, and measured steady-state ACh binding. Neither mutation affects K_{app} for ACh binding (Table II), showing that if these two residues form a salt bridge, it is unlikely to contribute to receptor function.

DISCUSSION

We show that three conserved residues at the periphery of the ACh binding site, αK145, αD200, and αY190, contribute profoundly to gating of the receptor channel. One of these residues, αY190, contributes to the aromatic cage that coordinates the quaternary ammonium moiety of the agonist (Celie et al., 2004), and its hydroxyl group projects away from the binding site toward the other two members of the triad (Fig. 1). Of the other two residues, αK145 is the most likely contact for αY190, but this contact corresponds to the agonist-bound conformation. Evidence for this contact comes from the AChBP crystal structure with CCh bound, which shows a salt bridge between the equivalent residues K139 and Y185 (Celie et al., 2004), and from the interdependent contributions of αK145 and αY190 to gating shown here. Support for electrostatic contact between αK145 and αD200 comes from the AChBP crystal structure without bound agonist, which shows a salt bridge between the equivalent Lys and Asp residues (Brejc et al., 2001), and from our data demonstrating interdependence of αK145 and αD200 in contributing to channel gating.

Our findings combine with inter-atomic distances in AChBP to suggest how interplay among these three residues couples local conformational change due to agonist binding to gating of the channel. Our inferences draw from two sets of atomic coordinates of AChBP with bound CCh deposited in the protein data bank (PDB code 1UV6): a pentameric unit with one molecule of CCh bound and another unit with two molecules of CCh bound. Inspection of the three subunit interfaces to which CCh is bound shows that recognition domain C is drawn inward toward the center of the binding site, whereas inspection of one of the unoccupied interfaces shows that domain C is extended outward from the site. Molecular dynamics simulation of AChBP and measurements of intrinsic tryptophan fluorescence reveal similar changes in the conformations of domain C with and without bound agonist (Gao et al., 2005). In the following mechanistic interpretation, we refer to these conformations as agonist-free and agonist-bound.

To illustrate our structural interpretation, the agonist-free and -bound conformations of recognition domain C of AChBP are compared (Fig. 12). The agonist-bound conformation is that of the crystal structure of AChBP with bound CCh (Celie et al., 2004). The agonist-free conformation is that generated by prolonged molecular dynamics simulation of AChBP (Gao et al., 2005), which is similar to the extended conformation of a subunit of AChBP at an unoccupied interface (see PDB entry 1UV6). ACh is shown docked in the orientation obtained by computational docking to the HEPES-bound crystal structure of AChBP (Brejc et al., 2001; Gao et al., 2005). In the agonist-free conformation, the Tyr at the position equivalent to αY190 is 8 Å away from the Lys equivalent to αK145, while residues equivalent to αK145 and αD200 form a salt bridge. In the agonist-bound conformation, the Tyr equivalent to αY190 moves to within 2–3 Å of the Lys equivalent to αK145, drawing recognition domain C inward, and allowing the residue equivalent to αD200 to move away from the Tyr/Lys pair. Thus by analogy to AChBP, in the resting state of the receptor, αK145 and αD200 are proposed to pair through electrostatic forces and αY190 is out of register (Fig. 11). However when the agonist binds, αY190 is drawn toward the αK145/αD200 pair and, through electrostatic forces, pulls αK145 away from αD200, allowing both residues to relax to new positions. These local inter-residue displacements could propagate to the channel via β-strands 7 and 10 of the ligand binding domain. β-Strand 7 harbors αK145 and forms part of the signature Cys-loop, which interacts with the linker spanning the M2 and M3 transmembrane domains (Kash et al., 2003; Bouzat et al., 2004), while β-strand 10 contains αD200 and links directly to the M1 transmembrane domain.

Although all three residues of the triad contribute profoundly to channel gating, each has a distinct role in linking the binding site to the channel. αY190 is the clear link to the ACh binding site, as shown by site-

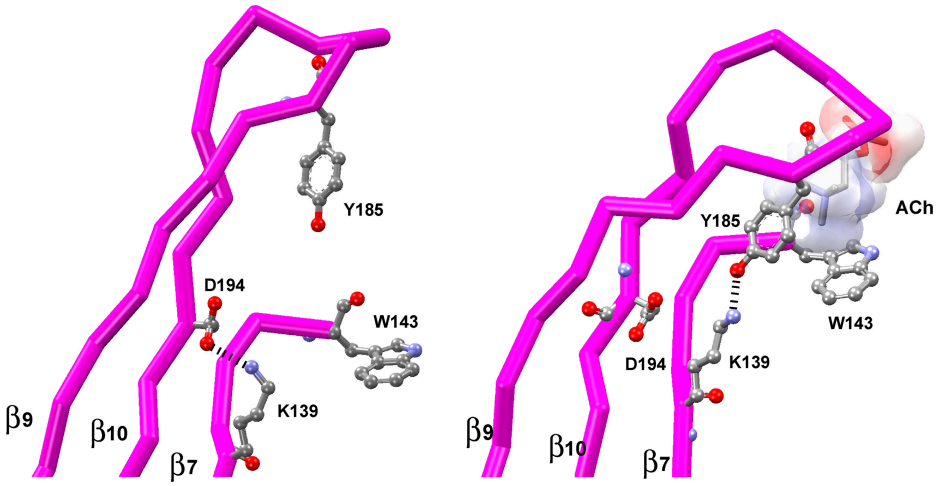

Figure 12. Structural interpretation. Agonist-free and agonist-bound conformations of recognition domain C of AChBP are compared. The triad of conserved residues is shown in stick representation. The agonist-free conformation is that generated by prolonged molecular dynamics simulation of AChBP (Gao et al., 2005), while the agonist-bound conformation is that of the crystal structure of AChBP with bound CCh (Celie et al., 2004). ACh is docked in the orientation obtained by computational docking to the HEPES-bound crystal structure of AChBP (Brejc et al., 2001; Gao et al., 2005). ACh is proposed to induce collapse of recognition domain C through aromatic-cation interactions, allowing Y185 to establish a salt bridge with K139 and weaken the K139/D194 salt bridge. The resulting displacements of β-strands 7 and 10 are proposed to propagate to channel and trigger opening. Putative salt bridges are indicated by dashes.

directed labeling (Abramson et al., 1989) and its location in the aromatic cage that coordinates the agonist (Celie et al., 2004). Its function is to help draw recognition domain C toward the center of the binding site when the agonist is bound and, in the process, form a salt bridge with αK145. Accordingly, removal of the aromatic hydroxyl group by mutation to Phe would prevent formation of the salt bridge and disrupt coupling of binding to gating. Likewise, substitution of Gln, Ala, or Glu for αK145 would remove the electrostatic partner for αY190, also disrupting coupling. By analogy to AChBP in the agonist-free conformation, αD200 is proposed to form a salt bridge with αK145, positioning αK145 for contact with the incoming αY190 and maintaining β-strands 7 and 10 in their closed state conformations. When the agonist binds, αY190 draws αK145 away from αD200, allowing β-strands 7 and 10 to move to their active conformations. Substitution of Asn for αD200 would prevent stabilization of αK145 for the incoming αY190, and break the link between β-strand 10 and the binding site, disrupting coupling.

One of the main lines of evidence that the triad identified here is an initial link in the binding to gating cascade is that mutation of each residue profoundly impairs gating of the channel. However two additional observations require explanation. First, the allosteric link between binding and gating domains is not completely disrupted by any of the mutations, as ACh can still trigger opening of the channel, although with greatly reduced efficiency. The most likely explanation is there are additional allosteric links that remain intact in each mutant receptor and account for the residual ACh-evoked currents. Second, the extent to which gating is disrupted differs by as much as 10-fold among the three mutations. If each member of the triad is essential for coupling, the extent to which gating is disrupted should be the same following mutation of each member. However in addition to coupling binding to gating, the triad may also contribute to the allosteric equilibrium between resting and open channel states in the absence of agonist (Jackson, 1989). This contribution to the allosteric set point likely involves dynamic interplay among the three residues, such that changes in the set point differ when one of the members is structurally altered. Thus for each mutation, the gating equilibrium for di-liganded receptors could be altered by differing amounts, owing to different contributions to the allosteric set point.

Other residues that contribute to the allosteric set point have been identified in the ligand binding domains of members of the Cys-loop receptor superfamily. In the nicotinic receptor α_1 subunit, mutation of Asp 97 markedly increases the frequency of channel opening events in the absence of ACh (Chakrapani et al., 2003). In the $GABA_A$ receptor ρ_1 subunit, mutation of Tyr 107 increases the resting membrane conductance in a manner that was sensitive to the specific GABA receptor inhibitor picrotoxin (Torres and Weiss, 2002). Similarly in the $GABA_A$ receptor β_2 subunit, mutation of Glu 155 increases the resting conductance in a picrotoxin-sensitive manner (Newell et al., 2004). In all three cases, the allosteric set point was increased in favor of the open channel state, whereas mutation of any residue of the triad in the present study impedes opening of the channel. Thus among functionally key residues in the ligand binding domain of the receptor, a balance is likely established between residues that promote and those that impair channel gating.

The triad of residues identified here is found in all species of nicotinic receptor α_1 subunits, suggesting

they contribute to agonist binding transduction in all muscle type nicotinic receptors (for subunit sequences see Le Novere and Changeux, 2001). Similarly, the triad is also present in all neuronal nicotinic α subunits (α_2–α_{10}), except α_5, which contains Asp at the position equivalent to αY190, and α_{10}, which contains Thr at the position equivalent to αK145. However, neither of these exceptions likely forms the principal face of the binding site; α_5 appears to be a structural subunit, requiring both neuronal α and β subunits to form functional receptors (Ramirez-Latorre et al., 1996), and α_{10} requires coexpression of the α_9 subunit (Sgard et al., 2002). On the other hand, the triad is not present in $GABA_A$, glycine, and 5-HT receptors. Thus among the Cys-loop superfamily of receptors, the initial coupling mechanism is likely to be highly similar for muscle and neuronal nicotinic receptors, but the more evolutionary distant receptors evolved different structures to relay the initial consequences of agonist binding. This structural divergence among receptors activated by different neurotransmitters is not surprising because the different agonist structures inherently require different chemical counterparts in the binding site.

In summary, our observations lead to identification of a triad of conserved residues as an initial link that couples agonist binding to channel gating. All three residues of the triad localize to the same three-dimensional region of our structural model of the receptor ligand binding domain, and all three residues are conserved across α_1 subunits. Also, equivalent residues in AChBP change conformation when the agonist is bound. Finally, structurally conservative mutations of each residue predominantly impair channel gating, and two pairs within the triad, αK145/αD200 and αK145/αY190, are interdependent in contributing to gating. Our findings suggest future studies aimed at identifying additional links that couple agonist binding to channel gating.

We thank Dr. Hai-Long Wang for the homology model and Fan Gao for the coordinates used to make Fig. 12.

This work was supported by National Institutes of Health grant NS31744 to S.M. Sine.

Olaf S. Andersen served as editor.

Submitted: 9 March 2005
Accepted: 5 May 2005

REFERENCES

Abramson, S.N., Y. Li, P. Culver, and P. Taylor. 1989. An analog of lophotoxin reacts covalently with tyrosine 190 in the α subunit of the nicotinic receptor. *J. Biol. Chem.* 264:12666–12672.

Akk, G., S. Sine, and A. Auerbach. 1996. Binding sites contribute unequally to the gating of mouse nicotinic αD200N acetylcholine receptors. *J. Physiol.* 496:185–196.

Bouzat, C., F. Gumilar, G. Spitzmaul, H.-L. Wang, D. Rayes, S.B. Hansen, P. Taylor, and S.M. Sine. 2004. Coupling of agonist binding to channel gating in an ACh-binding protein linked to an ion channel. *Nature.* 430:896–900.

Brejc, K., W. van Dijk, R. Klassen, M. Schuurmans, J. van der Oost, A. Smit, and T. Sixma. 2001. Crystal structure of an ACh-binding protein reveals the ligand-binding domain of nicotinic receptors. *Nature.* 411:269–276.

Celie, P., S. van Rossum-Fikkert, W. van Dijk, K. Brejc, A. Smit, and T. Sixma. 2004. Nicotine and carbamylcholine binding to nicotinic acetylcholine receptors as studied in AChBP crystal structures. *Neuron.* 41:907–914.

Chakrapani, S., T.D. Bailey, and A. Auerbach. 2003. The role of loop 5 in acetylcholine receptor channel gating. *J. Gen. Physiol.* 122:521–539.

Chakrapani, S., T.D. Bailey, and A. Auerbach. 2004. Gating dynamics of the acetylcholine receptor extracellular domain. *J. Gen. Physiol.* 123:341–356.

Chen, J., Y. Zhang, G. Akk, S. Sine, and A. Auerbach. 1995. Activation kinetics of recombinant mouse nicotinic acetylcholine receptors with mutations at α subunit residue tyrosine 190. *Biophys. J.* 69:849–859.

Colquhoun, D., and D.C. Ogden. 1988. Activation of ion channels in the frog end-plate by high concentrations of acetylcholine. *J. Physiol.* 395:131–159.

Colquhoun, D., and F. Sigworth. 1983. Fitting and statistical analysis of single channel records. *In* Single Channel Recording. B. Sakmann and E. Neher, editors. Plenum Publishing Corp., New York. 191–264.

Corringer, J.P., N. LeNovere, and J.P. Changeux. 2000. Nicotinic receptors at the amino acid level. *Annu. Rev. of Toxicol.* 40:431–458.

Elenes, S., and A. Auerbach. 2002. Desensitization of diliganded mouse muscle nicotinic acetylcholine receptor channels. *J. Physiol.* 541:367–383.

Gao, F., T. Burghardt, N. Bren, S.B. Hansen, R. Henchman, P. Taylor, J.A. McCammon, and S.M. Sine. 2005. Acetylcholine-mediated conformational changes in acetylcholine-binding protein revealed by simulation and intrinsic tryptophan fluorescence. *J. Biol. Chem.* 280:8443–8451.

Hamill, O.P., A. Marty, E. Neher, B. Sakmann, and F.J. Sigworth. 1981. Improved patch-clamp techniques for high-resolution current recording from cells and cell-free membrane patches. *Pflugers Arch.* 391:85–100.

Hatton, C.J., C. Shelley, M. Brydson, D. Beeson, and D. Colquhoun. 2003. Properties of the human muscle nicotinic receptor, and of the slow-channel myasthenic syndrome mutant εL221F, inferred from maximum likelihood fits. *J. Physiol.* 547:729–760.

Horovitz, A., and A.R. Fersht. 1990. Strategy for analysing the cooperativity of intramolecular interactions in peptides and proteins. *J. Mol. Biol.* 214:613–617.

Jackson, M.B. 1989. Perfection of a synaptic receptor: kinetics and energetics of the acetylcholine receptor. *Proc. Natl. Acad. Sci. USA.* 86:2199–2203.

Karlin, A. 2002. The emerging structure of the nicotinic acetylcholine receptors. *Nat. Rev. Neurosci.* 3:102–114.

Kash, T., A. Jenkins, J. Kelly, J. Trudell, and N.L. Harrison. 2003. Coupling of agonist binding to channel gating in the $GABA_A$ receptor. *Nature.* 421:272–275.

Katz, B., and S. Thesleff. 1957. A study of desensitization produced by acetylcholine at the motor end-plate. *J. Physiol.* 138:63–80.

Le Novere, N., and J.P. Changeux. 2001. LGICdb: the ligand-gated ion channel database. *Nucleic Acids Res.* 29:294–295.

Le Novere, N., T. Grutter, and J.P. Changeux. 2002. Models of the extra-cellular domain of the nicotinic receptors and of agonist- and Ca^{2+}-binding sites. *Proc. Natl. Acad. Sci. USA.* 99:3210–3215.

Lee, B.S., R.B. Gunn, and R.R. Kopito. 1991. Functional differences among nonerythroid anion exchangers expressed in a trans-

fected human cell line. *J. Biol. Chem.* 266:11448–11454.

Lee, W.Y., and S.M. Sine. 2004. Invariant aspartic acid in muscle nicotinic receptor contributes selectively to the kinetics of agonist binding. *J. Gen. Physiol.* 124:555–567.

Milone, M., H.L. Wang, K. Ohno, R. Prince, T. Fukudome, X.M. Shen, J.M. Brengman, R.C. Griggs, S.M. Sine, and A.G. Engel. 1998. Mode switching kinetics produced by a naturally occurring mutation in the cytoplasmic loop of the human acetylcholine receptor epsilon subunit. *Neuron.* 20:575–588.

Miyazawa, A., Y. Fujiyoshi, and N. Unwin. 2003. Structure and gating mechanism of the acetylcholine receptor pore. *Nature.* 423: 949–955.

Molles, B.E., I. Tsigelny, P. Nguyen, S. Gao, S.M. Sine, and P. Taylor. 2002. Residues in the ε subunit of the nicotinic acetylcholine receptor interact to confer selectivity of Waglerin-1 for the α–ε subunit interface site. *Biochemistry.* 41:7895–7906.

Newell, J.G., R.A. McDevitt, and C. Czajkowski. 2004. Mutation of glutamate 155 of the GABA(A) receptor β2 subunit produces a spontaneously open channel: a trigger for channel activation. *J. Neurosci.* 24:11226–11235.

Ohno, K., H.-L. Wang, M. Milone, N. Bren, J.M. Brengman, S. Nakano, P. Quiram, J.N. Pruitt, S.M. Sine, and E.G. Engel. 1996. Congential myasthenic syndrome caused by decreased agonist binding affinity due to a mutation in the acetylcholine receptor ε subunit. *Neuron.* 17:157–170.

Pear, W.S., G.P. Nolan, M.L. Scott, and D. Baltimore. 1993. Production of high-titer helper-free retroviruses by transient transfection. *Proc. Natl. Acad. Sci. USA.* 90:8392–8396.

Schapira, M., R. Abagyan, and M. Totrov. 2002. Structural model of nicotinic acetylcholine receptor isotypes bound to acetylcholine and nicotine. *BMC Struct. Biol.* 2:1.

Qin, F., A. Auerbach, and F. Sachs. 1996. Estimating single channel kinetic parameters from idealized patch clamp data containing missed events. *Biophys. J.* 70:264–280.

Ramirez-Latorre, J., C.R. Yu, X. Qu, F. Perin, A. Karlin, and L. Role. 1996. Functional contributions of α-5 subunit to neuronal receptors. *Nature.* 380:347–351.

Sakmann, B., J. Patlak, and E. Neher. 1980. Single acetylcholine-activated channels show burst-kinetics in presence of desensitizing concentrations of agonist. *Nature.* 286:71–73.

Sgard, F., E. Charpantier, S. Bertrand, N. Walker, D. Caput, D. Graham, D. Bertrand, and F. Besnard. 2002. A novel human nicotinic receptor subunit, α10, that confers functionality to the α9-subunit. *Mol. Pharmacol.* 61:150–159.

Sine, S.M., and J.H. Steinbach. 1987. Activation of acetylcholine receptors in clonal BC3H-1 cells by high concentrations of agonist. *J. Physiol.* 385:325–359.

Sine, S.M. 1993. Molecular dissection of subunit interfaces in the acetylcholine receptor: identification of residues that determine curare selectivity. *Proc. Natl. Acad. Sci. USA.* 90:9436–9440.

Sine, S.M., and P. Taylor. 1979. Functional consequences of agonist-mediated state transitions in the cholinergic receptor. *J. Biol. Chem.* 254:3315–3325.

Sine, S.M. 2002. The nicotinic receptor ligand binding domain. *J. Neurobiol.* 53:431–446.

Sine, S.M., H.L. Wang, and N. Bren. 2002a. Lysine scanning mutagenesis delineates structural model of the nicotinic receptor ligand binding domain. *J. Biol. Chem.* 277:29210–29223.

Sine, S.M., X.M. Shen, H.L. Wang, K. Ohno, W.Y. Lee, A. Tsujino, J. Brengmann, N. Bren, J. Vajsar, and A.G. Engel. 2002b. Naturally occurring mutations at the acetylcholine receptor binding site independently alter ACh binding and channel gating. *J. Gen. Physiol.* 120:483–496.

Torres, V.I., and D.S. Weiss. 2002. Identification of a tyrosine in the agonist binding site of the homomeric rho1 γ-aminobutyric acid (GABA) receptor that, when mutated, produces spontaneous opening. *J. Biol. Chem.* 277:43741–43748.

Unwin, N. 2005. Refined structure of the nicotinic acetylcholine receptor at 4 Å resolution. *J. Mol. Biol.* 346:967–989.

Wang, H.-L., M. Milone, K. Ohno, X.-M. Shen, A. Tsujuno, A. Paola, P. Tonali, J. Brengman, A.G. Engel, and S.M. Sine. 1999. Acetylcholine receptor M3 domain: stereochemical and volume contributions to channel gating. *Nat. Neurosci.* 2:226–233.

Wang, H.-L., K. Ohno, M. Milone, J.M. Brengman, A. Evoli, A.P. Batocchi, L.T. Middleton, K. Christodoulou, A.G. Engel, and S.M. Sine. 2000. Fundamental gating mechanism of nicotinic receptor channel revealed by mutation causing a congenital myasthenic syndrome. *J. Gen. Physiol.* 116:449–462.